

Mutant *KRAS*-driven cancers depend on *PTPN11*/*SHP2* phosphatase

Dietrich A. Ruess^{1,2}, Guus J. Heynen³, Katrin J. Ciecieski¹, Jiaoyu Ai¹, Alexandra Berninger¹, Derya Kabacaoglu¹, Kivanc Görgülü¹, Zahra Dantes¹, Sonja M. Wörmann¹, Kalliope N. Diakopoulos¹, Angeliki F. Karpathaki¹, Marlena Kowalska¹, Ezgi Kaya-Aksoy¹, Liang Song¹, Eveline A. Zeeuw van der Laan³, María P. López-Alberca⁴, Marc Nazaré⁴, Maximilian Reichert¹, Dieter Saur¹, Mert M. Erkan⁵, Ulrich T. Hopt², Bruno Sainz Jr⁶, Walter Birchmeier³, Roland M. Schmid¹, Marina Lesina¹ and Hana Algül^{1*}

The ubiquitously expressed non-receptor protein tyrosine phosphatase SHP2, encoded by *PTPN11*, is involved in signal transduction downstream of multiple growth factor, cytokine and integrin receptors¹. Its requirement for complete RAS-MAPK activation and its role as a negative regulator of JAK-STAT signaling have established SHP2 as an essential player in oncogenic signaling pathways^{1–7}. Recently, a novel potent allosteric SHP2 inhibitor was presented as a viable therapeutic option for receptor tyrosine kinase-driven cancers, but was shown to be ineffective in *KRAS*-mutant tumor cell lines *in vitro*⁸. Here, we report a central and indispensable role for SHP2 in oncogenic *KRAS*-driven tumors. Genetic deletion of *Ptpn11* profoundly inhibited tumor development in mutant *KRAS*-driven murine models of pancreatic ductal adenocarcinoma and non-small-cell lung cancer. We provide evidence for a critical dependence of mutant *KRAS* on SHP2 during carcinogenesis. Deletion or inhibition of SHP2 in established tumors delayed tumor progression but was not sufficient to achieve tumor regression. However, SHP2 was necessary for resistance mechanisms upon blockade of MEK. Synergy was observed when both SHP2 and MEK were targeted, resulting in sustained tumor growth control in murine and human patient-derived organoids and xenograft models of pancreatic ductal adenocarcinoma and non-small-cell lung cancer. Our data indicate the clinical utility of dual SHP2/MEK inhibition as a targeted therapy approach for *KRAS*-mutant cancers.

RAS genes constitute the most frequently mutated oncogene family in human cancers⁹. Although *KRAS* mutations are virtually universal in pancreatic ductal adenocarcinoma (PDAC), they occur in up to 30% of non-small-cell lung cancer (NSCLC)^{9,10}. Recently, genome-wide association analysis and functional characterization identified the long intergenic noncoding RNA LINC00673 as a potential tumor suppressor that acts through regulation of pre-mRNA-processing factor 19 (PRPF19)-mediated ubiquitination and degradation of SHP2 (encoded by *PTPN11*) in PDAC. The germline G > A variation at rs11655237 impairs this effect of LINC00673 and confers susceptibility to tumorigenesis¹¹, implying a

proto-oncogenic role for SHP2. In addition, SHP2 promotes RAS-RAF-MAP-kinase kinase (MEK)-extracellular signal-regulated kinase (ERK) signaling in NSCLC with epidermal growth factor receptor (EGFR)-activating mutations^{12,13}, but evidence for its relevance in *KRAS*-mutant NSCLC is lacking.

Oncogenomic database analysis together with protein expression profiling in several human PDAC and NSCLC tissues and cell lines revealed the epithelial presence of SHP2 (Supplementary Fig. 1a–e). As a sign of recruitment and activation, its Y542 phosphorylation^{14–16} was detected in a heterogeneous pattern in the majority of samples analyzed (Supplementary Fig. 1b–d). Transcriptional levels of *PTPN11* had no clear association with overall survival in The Cancer Genome Atlas (TCGA) RNA-seq PDAC and NSCLC (*KRAS*-mutant subgroup) data sets (Supplementary Fig. 1f,g). These results suggest that SHP2 activation, rather than expression levels, determines its action in PDAC and NSCLC.

To genetically dissect the contribution of SHP2 in PDAC and NSCLC tumorigenesis, we utilized oncogenic *KRAS*-driven murine cancer models, which allow for tissue-specific expression of the G12D mutation in *KRAS* (*KRAS*^{G12D}) and the initiation of tumors in the pancreas or lung^{17,18}. In both PDAC and NSCLC models, SHP2 expression was observed during the entire process of tumor development (Supplementary Fig. 2a–e). Pancreas-specific biallelic deletion of *Ptpn11* in *KRAS*^{G12D} mice (termed: *Kras*), but not mono-allelic deletion (data not shown), led to profound inhibition of pancreatic intraepithelial neoplasia (PanIN) development (Fig. 1a,b and Supplementary Fig. 3a), pancreatic enlargement (Supplementary Fig. 3b) and desmoplasia (Fig. 1a and Supplementary Fig. 3c). PDAC formation was almost completely blocked, and survival was dramatically prolonged when *Ptpn11* was deleted (Fig. 1c and Supplementary Fig. 3d). Likewise, inflammation-triggered acceleration of pancreatic carcinogenesis by cerulein was inhibited in the absence of SHP2 (Supplementary Fig. 3e–h). In an *ex vivo* acinar-to-ductal metaplasia assay¹⁹, genetic deletion and pharmacological inhibition revealed a requirement of SHP2 and its phosphatase activity for efficient acinar transdifferentiation (Supplementary Fig. 3i,j). Next, we took advantage of the more-aggressive and tumor-prone

¹Mildred-Scheel-Chair of Tumor Metabolism, Internal Medicine II, Klinikum rechts der Isar, Technische Universität München, Munich, Germany.

²Department of Surgery, Faculty of Medicine, Medical Center—University of Freiburg, Freiburg, Germany. ³Cancer Research Program, Max Delbrück Center for Molecular Medicine (MDC) in the Helmholtz Society, Berlin, Germany. ⁴Medicinal Chemistry, Leibniz-Forschungsinstitut für Molekulare Pharmakologie, Berlin, Germany. ⁵Koç University School of Medicine, Istanbul, Turkey. ⁶Department of Biochemistry, Autónoma University of Madrid, School of Medicine, Instituto de Investigaciones Biomédicas “Alberto Sols”, Madrid, Spain. *e-mail: hana.alguel@mri.tum.de

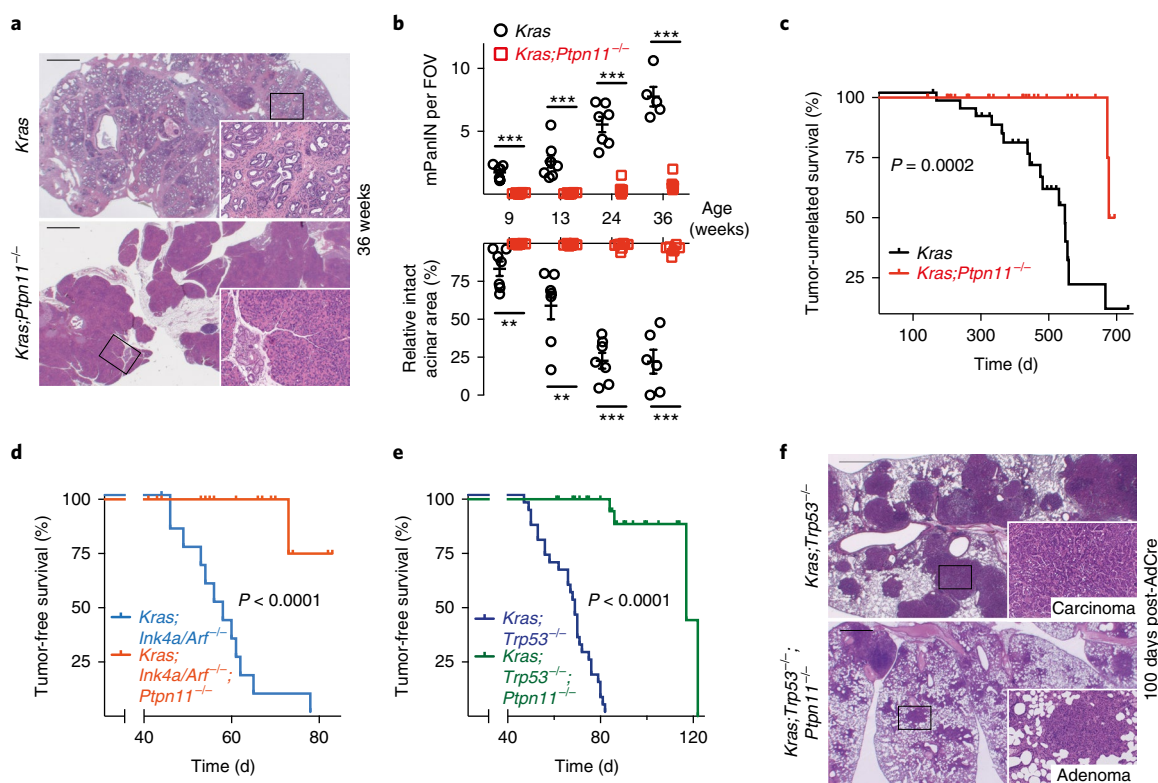


Fig. 1 | Loss of *Ptpn11* profoundly inhibits KRAS^{G12D}-driven pancreatic and pulmonary carcinogenesis. **a**, Representative H&E-stained sections of pancreata from *Kras* ($n=5$) and *Kras;Ptpn11*^{-/-} mice ($n=6$) at 36 weeks of age with similar results. Scale bars, 1,000 μm . Insets: magnification $\times 10$. **b**, Murine PanIN (mPanIN) development and the relative intact, untransformed acinar area in *Kras* and *Kras;Ptpn11*^{-/-} pancreata. Lesions and the acinar area were quantified over one whole H&E-stained pancreatic section from mice with the indicated age (13 weeks *Kras*, 24 weeks *Kras;Ptpn11*^{-/-}; $n=8$ animals; 9 and 24 weeks *Kras*: $n=7$ animals; 9, 13 and 36 weeks *Kras;Ptpn11*^{-/-}: $n=6$ animals; 36 weeks *Kras*: $n=5$ animals). FOV, field of view. Mean \pm s.e.m. is shown. *** $P < 0.001$; ** $P < 0.01$; unpaired, two-tailed Student's *t*-test. **c**, Kaplan–Meier analysis of tumor-unrelated survival of *Kras* mice ($n=32$, median: 548 d) and *Kras;Ptpn11*^{-/-} mice ($n=30$, median: 685.5 d). Ticks indicate censored mice that were euthanized for decline in clinical condition, but without microscopic evidence of PDAC. Details for all mice of the *Kras;Ptpn11*^{-/-} cohort are given in Supplementary Fig. 3d. Significance was determined by log-rank (Mantel–Cox) test. **d**, Kaplan–Meier analysis of tumor-free survival of *Kras;Ink4a/Arf*^{-/-} mice ($n=14$, median: 58 d) and *Kras;Ink4a/Arf*^{-/-};*Ptpn11*^{-/-} mice ($n=19$, median: undefined). Ticks indicate censored mice that were euthanized due to paraparesis, without histological evidence of more than rare low-grade PanIN in the pancreas (see Supplementary Fig. 4d for details). Significance was determined by log-rank (Mantel–Cox) test. **e**, Kaplan–Meier analysis of tumor-free survival of *Kras;Trp53*^{-/-} mice ($n=29$, median: 69 d) and *Kras;Trp53*^{-/-};*Ptpn11*^{-/-} mice ($n=28$, median = 117 d). Ticks indicate censored mice that were euthanized due to decline in clinical condition, without histological evidence of PDAC (see Supplementary Fig. 4c for details). Significance was determined by log-rank (Mantel–Cox) test. **f**, Lung adenocarcinoma model: *Ptfla*^{Cre-ex1} was replaced by transnasal inhalation of AdCre. Representative H&E micrographs of lungs from *Kras;Trp53*^{-/-} and *Kras;Trp53*^{-/-};*Ptpn11*^{-/-} mice 100 days after AdCre inhalation, illustrating the difference in tumor development and tumor load; *Kras;Trp53*^{-/-} ($n=14$) versus *Kras;Trp53*^{-/-};*Ptpn11*^{-/-} ($n=16$) animals in the whole survival analysis cohorts with similar results. The mice shown here were chosen for demonstrative reasons given their equal survival time. Scale bars, 1,000 μm . Insets: magnification $\times 10$.

PDAC mouse models with loss of *Ink4a/Arf*²⁰ or monoallelic/biallelic deletion of *Trp53* (ref. ²¹). Strikingly, even in these backgrounds, *Ptpn11* deficiency potentially blocked PanIN progression and PDAC development, translating into significant and extended tumor-free survival (Fig. 1d,e and Supplementary Fig. 4a). Only a few macroscopic tumors were detected in *Kras;Trp53*^{-/-};*Ptpn11*^{-/-} or *Kras;Trp53*^{-/-};*Ptpn11*^{-/-} mice and none in *Kras;Ink4a/Arf*^{-/-};*Ptpn11*^{-/-} mice (Supplementary Fig. 4b–d). Comparable observations were made in a KRAS^{G12D}-driven model of NSCLC. The pulmonary ‘atypical adenomatous hyperplasia–adenoma–adenocarcinoma’ progression sequence was significantly delayed in the absence of *Ptpn11* (Supplementary Fig. 5a–c,f). Even in the more-rapid *Kras;Trp53*^{-/-} context, loss of *Ptpn11* resulted in a substantial deceleration of NSCLC disease dynamics and reduced tumor burden, which translated into considerably prolonged survival (Fig. 1f and Supplementary Fig. 5d,e,g,h). Of note, unlike in the PDAC models, a substantial fraction of tumors that emerged in the NSCLC models demonstrated escape from *Ptpn11* deletion (Supplementary Fig. 5i).

Taken together, these in vivo data indicate a central and indispensable role for SHP2 in carcinogenesis of oncogenic KRAS-driven epithelial tumors of the pancreas and lung.

Formation of preneoplastic lesions and progression to carcinoma in these KRAS^{G12D}-driven models correlates with enhancement of RAF–MEK–ERK signaling^{22,23}. However, phosphorylation of ERK in early-transforming *Kras* pancreata or lungs was greatly diminished in *Kras;Ptpn11*^{-/-} mice (Fig. 2a and Supplementary Figs. 5j,k and 6a). In addition, the direct and indirect oncogenic RAS-effector phosphatidylinositol-3-OH kinase (PI3K)–AKT and signal transducer and activator of transcription 3 (STAT3) pathways were not activated in transforming *Kras*, but not in *Kras;Ptpn11*^{-/-} pancreata (Fig. 2a). Considerably decreased levels of RAF–RAS-binding domain (RBD)-bound pan-RAS as well as RBD-bound KRAS^{G12D} in tissue lysates of *Kras;Ptpn11*^{-/-} pancreata (Fig. 2b) suggested severe RAS signaling defects upon *Ptpn11* deletion. To gain a more comprehensive insight into the impact of abrogated *Ptpn11* in KRAS^{G12D}-expressing pancreata, we performed transcriptomics

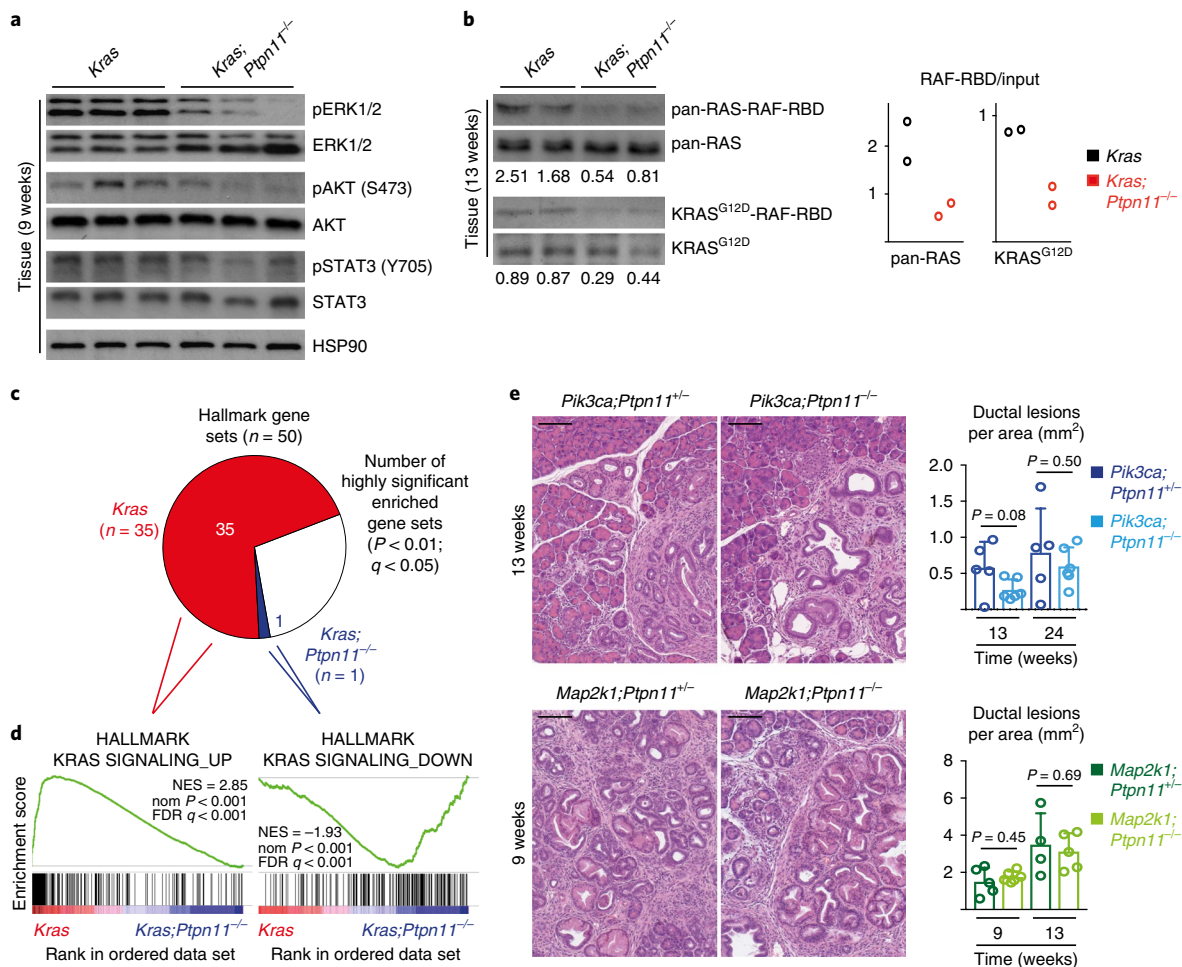


Fig. 2 | Oncogenic KRAS depends on SHP2 for adequate activity during carcinogenesis. **a**, Immunoblot with lysates from pancreatic tissue (9-week-old mice) of *Kras* and *Kras;Ptpn11^{-/-}* animals using the specific antibodies indicated. Three biologically independent samples per group are shown. HSP90 served as the loading control. Full scan images are shown in Supplementary Fig. 18a. **b**, RAF-RBD agarose affinity precipitation experiments of representative samples (two biologically independent samples per group) from pancreatic tissue (13-week-old mice) with the *Kras* and *Kras;Ptpn11^{-/-}* genotypes. Pull-down of RAS-GTP was performed with commercially available RAF-RBD agarose beads. Precipitates were immunoblotted using a pan-RAS (labeled: pan-RAS-RAF-RBD)- or a mutant KRAS^{G12D}-specific antibody (labeled: KRAS^{G12D}-RAF-RBD). Immunoblots of the input samples with the identical antibodies are displayed below (labeled: pan-RAS and KRAS^{G12D}, respectively). Numerical values indicate the ratio of densitometrically quantified signals from pull-down over input samples. Ratios are illustrated by the panels on the right. For uncropped images, including molecular weight markers, see Supplementary Fig. 18b. **c, d**, GSEA of mRNA microarray data from pancreatic tissue samples of 9-week-old *Kras* and *Kras;Ptpn11^{-/-}* mice ($n = 3$ animals per group); analysis and statistics were performed using GSEA software provided by the Broad Institute, as previously described⁴². **c**, The pie chart illustrates the fractions of highly significant enriched gene sets in the ‘Hallmark’ collection in *Kras* versus *Kras;Ptpn11^{-/-}* samples. The white pie piece represents non-significant gene sets. **d**, Enrichment plots for KRAS signaling signatures from the ‘Hallmark’ gene set collection. Left: one of the most significantly enriched gene sets in *Kras* samples (genes upregulated by KRAS signaling are enriched in *Kras*); right: the unique enriched gene set in *Kras;Ptpn11^{-/-}* samples (genes downregulated by KRAS signaling are enriched in *Kras;Ptpn11^{-/-}*). FDR, false discovery rate; NES, normalized enrichment score; nom, nominal. **e**, Representative H&E micrographs of SHP2-proficient (*Ptpn11^{+/-}*) versus SHP2-deficient (*Ptpn11^{-/-}*) pancreatic epithelia at the indicated time points expressing constitutively active mutant PI3KCA (upper panel; R26-LSL-*Pik3ca*^{H1047R}, *Ptf1a*^{Cre-ex1}) or MEK1 (lower panel; R26-LSL-*Map2k1*^{S218D/S222D}, *Ptf1a*^{Cre-ex1}). Scale bars, 100 μ m. Quantification of ductal lesions (acinar-to-ductal metaplasia + PanIN) was performed on one whole-tissue section per mouse and is displayed as bar graphs on the right. 13 and 24 weeks *Pik3ca;Ptpn11^{-/-}* and 9 weeks *Map2k1;Ptpn11^{-/-}*: $n = 6$ mice; 13 and 24 weeks *Pik3ca;Ptpn11^{+/-}*, 13 weeks *Map2k1;Ptpn11^{-/-}* and 9 weeks *Map2k1;Ptpn11^{+/-}*: $n = 5$ mice; 13 weeks *Map2k1;Ptpn11^{+/-}*: $n = 4$ mice. Mean \pm s.d. is shown. Significance was determined by unpaired, two-tailed Student’s *t*-test.

on pancreatic tissue samples from 9-week-old mice. Gene set enrichment analysis (GSEA) revealed a remarkably skewed pattern of significantly enriched gene sets in favor of *Kras* compared to *Kras;Ptpn11^{-/-}* samples (Fig. 2c and Supplementary Fig. 6b,c). Enriched gene sets in *Kras* tissue included established oncogenic facets, such as increased transcriptional activity, transdifferentiation, cell stress and altered metabolism, as well as inflammation, desmoplasia and (re-)activation of embryonic signaling cascades

(Supplementary Fig. 6b–f). More importantly, a clear loss of a KRAS signaling signature was evident in *Kras;Ptpn11^{-/-}* samples (Fig. 2d). Consequently, and consistent with the findings in Fig. 2a, signatures related to pathways that are known to be directly or indirectly linked to oncogenic KRAS, such as MEK, AKT and interleukin-6 (IL-6)–Janus kinase (JAK)–STAT3 signaling were lost with *Ptpn11* deletion (Supplementary Fig. 6h). In addition, *Kras* samples demonstrated enrichment of signatures of multiple growth factors,

receptor tyrosine kinases (RTKs) and immediate signal transducers upstream of RAS, suggesting a SHP2-dependent positive-feedback loop for amplification of RAS activity above an oncogenic threshold²⁴ (Supplementary Fig. 6g). To further demonstrate the dependency of oncogenic KRAS on SHP2 in pancreatic carcinogenesis, we first bred *Ptpn11* mice with MAP2K1^{DD} or PI3KCA^{H1047R} mice^{25,26}. These crossings revealed that *Ptpn11* is redundant in the presence of constitutively active mutant MEK1 or PI3K (Fig. 2e) and, therefore, SHP2 functions upstream, at the level of KRAS. Given the pleiotropic regulatory effects of SHP2 on signaling pathways, and its inhibitory role in the STAT3 pathway in particular⁶, we further utilized a previously published KRAS^{G12D} mouse model lacking the negative-feedback STAT3 regulator SOCS3 specifically in the pancreas (*Kras;Socs3*^{-/-})²⁷. Loss of *Ptpn11* in this model did not further aggravate but rescued the aggressive STAT3-dependent phenotype of PDAC development (Supplementary Fig. 7a–c), suggesting a requirement of SHP2 for inflammatory, paracrine oncogenic circuits, elicited by KRAS^{G12D} and mediated by STAT3 (ref. 27). These genetic in vivo data demonstrate a dominant upstream role for SHP2 in regulating both adequate activity and oncogenic potency of KRAS^{G12D} in pancreatic carcinogenesis.

To examine the contribution of SHP2 in tumor maintenance, we utilized a dual-recombinase approach²⁸: mice with pancreas-specific Flippase-mediated recombination (*Pdx-Flpo*) of *FSF-Kras*^{G12D/+} and *Trp53*^{tr/trl} alleles were monitored with magnetic resonance imaging (MRI) for tumor occurrence. Upon tumor detection, deletion of *Ptpn11* was achieved by a tamoxifen-inducible Cre-recombinase, which was expressed exclusively in the Flpo-recombined epithelial PDAC compartment (*FSF-CreRT*). Subsequently, tumor dynamics were evaluated weekly with MRI (Fig. 3a). These experiments revealed that deletion of *Ptpn11* in established murine PDAC epithelia was not sufficient to achieve tumor regression or prolong survival, but led to slower tumor growth and reduced pan-RAS and KRAS^{G12D} activity levels in vivo and in vitro; tumor morphology was unchanged (Fig. 3b–e and Supplementary Fig. 8a–h).

In line with this finding, clustered regularly interspaced short palindromic repeats (CRISPR)–CRISPR-associated protein 9 (Cas9)-mediated knockout of *PTPN11* in two KRAS-mutant human PDAC cell lines (YAPC: KRAS^{G12V}; PANC-1: KRAS^{G12D}) resulted in reduced in vitro proliferation (with serum-rich 10% FBS conditions), delayed tumor growth in an in vivo xenograft setting and diminished RBD-bound KRAS levels (Supplementary Fig. 8i–l).

Aiming to identify pharmacological vulnerabilities conferred by loss of SHP2, we performed a focused drug screen with *PTPN11*-knockout cells using PDAC- and NSCLC-relevant chemotherapeutics (gemcitabine, oxaliplatin and paclitaxel) and selected small molecules targeting RAS downstream effector kinases (PI3K and MEK). These experiments revealed that *PTPN11*-knockout cells were uniquely susceptible to MEK inhibitors (Fig. 3f and Supplementary Fig. 9a,b). Intrinsic and acquired resistance to MEK inhibition is a common phenomenon that has been attributed to activation of RTK signaling in KRAS-mutant and BRAF-mutant contexts^{29–34}. Thus, MEK inhibitors have failed to enter into the clinic as a single adjunct to conventional chemotherapy in PDAC and NSCLC^{35,36}. The KRAS-mutant human PDAC cell lines YAPC, PANC-1 and DAN-G are relatively resistant to MEK inhibition, whereas CAPAN-2 is sensitive to MEK inhibition (Supplementary Fig. 10a). After prolonged treatment with selumetinib (a MEK inhibitor), the phosphorylation levels of ERK increased steadily over time, reaching near to the untreated control levels in YAPC, PANC-1 and DAN-G cells, whereas CAPAN-2 cells were incapable of reactivating ERK (Supplementary Fig. 10b). In parallel, we observed phosphorylation of multiple RTKs, strong Y542 phosphorylation and increased phosphatase activity of SHP2 upon treatment with selumetinib (Fig. 3g and Supplementary Fig. 10b–f), suggesting that SHP2 transmits a RTK-mediated feedback loop, conferring

resistance to MEK inhibitors. Indeed, YAPC and PANC-1 *PTPN11*-knockout cells were incapable of reactivating mitogen-activated protein kinase (MAPK) signaling in the presence of selumetinib (Fig. 3h and Supplementary Fig. 10g). Reconstitution of wild-type SHP2 or phosphatase-dead SHP2^{C459S} in the *PTPN11*-knockout cells demonstrated the requirement of SHP2 phosphatase activity for restoration of MAPK signaling and proliferative capacity in response to selumetinib (Supplementary Fig. 11a,b). As these results provided a strong rationale for a dual SHP2/MEK inhibition, we targeted SHP2 in co-inhibition assays with two different compounds that have been previously characterized in detail: the catalytic-site inhibitor GS493 (ref. 37) or the recently reported compound SHP099 (refs 8,38), which allosterically stabilizes SHP2 in its closed autoinhibited conformation³⁸. Their different modes of action were confirmed in a *PTPN11*-knockout PANC-1 cell line, reconstituted with the SHP2^{E76A} mutation, which perturbs autoinhibition and thus renders the allosteric inhibitor ineffective (Supplementary Fig. 11c). Both compounds phenocopied the effect seen in *PTPN11*-knockout cells and demonstrated remarkable synergism with the MEK inhibitors selumetinib and trametinib in multiple murine and human PDAC and NSCLC cell lines. In addition, GS493 and SHP099 showed synergistic potential in combination with PI3K inhibitors, but not with conventional chemotherapeutics (Fig. 3i and Supplementary Figs. 11d–h and 12a,b). The panels in Supplementary Fig. 13a,b demonstrate that synergism of combined SHP2/MEK inhibition is not only restricted to the KRAS mutant but is also evident in various KRAS wild-type tumor cell lines.

To test the translational relevance of our findings, we set up three levels of experiments. We first treated endogenous PDAC-bearing *Kras;Trp53*^{-/-} mice with GS493, trametinib or in combination. Similar to the results with human cell line xenotransplants (Supplementary Fig. 8l), GS493 alone only modestly inhibited tumor progression. As reported for selumetinib³⁹, trametinib, which possesses superior pharmacodynamics compared to other MEK inhibitors⁴⁰, achieved initial pancreatic volume reduction, but eventually, resistant tumors emerged. However, co-treatment with trametinib + GS493 impeded resistance dynamics and achieved sustained tumor growth inhibition (Fig. 4a,b and Supplementary Fig. 14a–d). Similar potent effects were observed with NSCLC-bearing *Kras;Trp53*^{-/-} adenoviral Cre (AdCre) mice, where marked total lesion volume regression was obtained with dual SHP2/MEK inhibition (Fig. 4c and Supplementary Fig. 15a–e). In line with previous observations, co-inhibition resulted in sustained reduction of ERK phosphorylation and decreased tumor proliferation in both models (Supplementary Figs. 14e,f and 15f,g). Second, primary patient-derived ex vivo KRAS-mutant PDAC organoids exhibited reduced half-maximum inhibitory concentration (IC₅₀) values for trametinib upon addition of SHP099 (Fig. 4d and Supplementary Fig. 16). Last, patient-derived KRAS^{G12D} tumor tissue xenografts demonstrated *in vivo* susceptibility to combined SHP2/MEK inhibition (Fig. 4e,f and Supplementary Fig. 17a–d). As illustrated with PDAC ID_02, trametinib induced the enhancement of pan-RAS and KRAS^{G12D} activity as well as the PI3K pathway; however, in the dual treatment arm, these effects were constrained, culminating in significantly reduced proliferation, elevated cleaved caspase 3 levels and complete growth inhibition. Of note, SHP2 inhibition did not have detrimental effects on STAT3 phosphorylation. Taken together, these results demonstrate a potent synergistic effect of combined SHP2 and MEK inhibition in KRAS-mutant carcinomas.

Although SHP2 has been considered to be dispensable for mutated oncogenic KRAS function⁸, using mouse and human pancreatic and lung cancer models combined with genetic and pharmacological inhibition approaches, our data indicate that oncogenic KRAS activity depends on SHP2 for its intensification and for downstream signaling during carcinogenesis. In established tumors, loss or inhibition of SHP2 decelerates tumor progression and, more

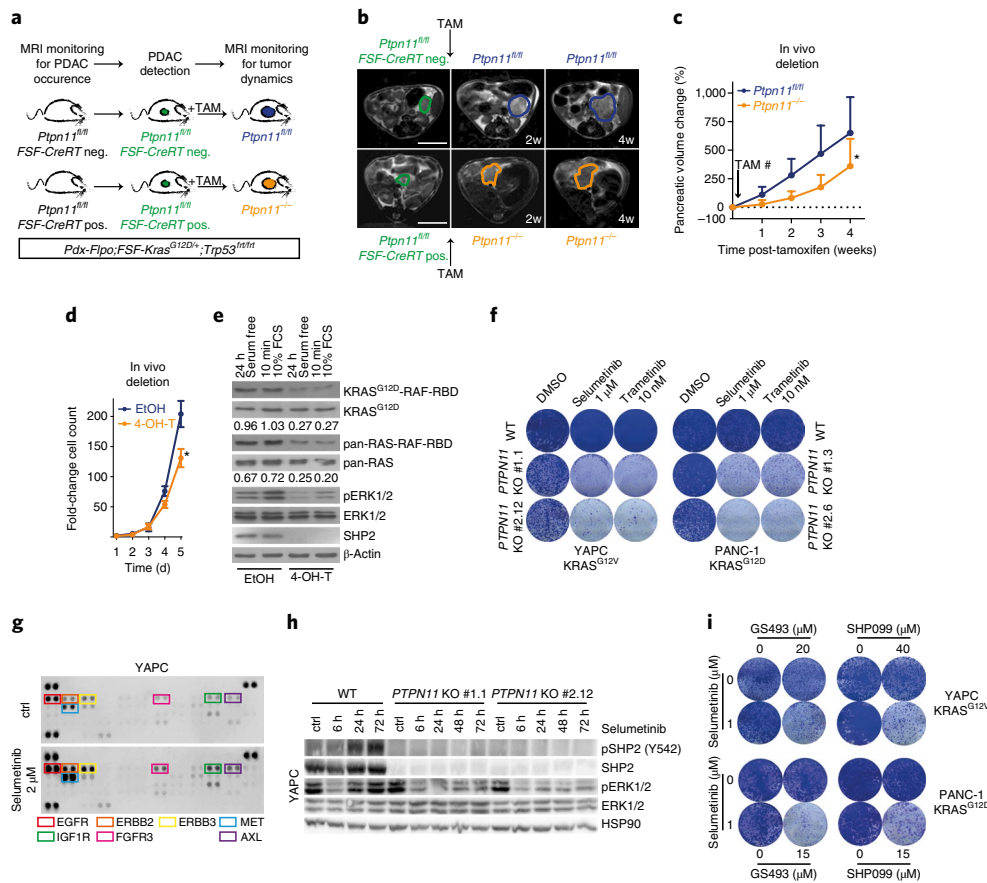


Fig. 3 | Loss of SHP2 in established PDAC decelerates tumor progression and sensitizes to MEK inhibition. **a**, Schematic of the experimental workflow with the dual-recombinase PDAC model. Pancreatic tumors arise in *Pdx-Flo;Kras^{FSF-G12D/+};Trp53^{fl/fl};R26^{FSF-CAG-CreERT2}* (positive or negative); *Ptpn11^{fl/fl}* mice, which are genetically engineered to allow a temporospatially controlled second recombination event through a tamoxifen (TAM)-inducible Cre-recombinase, expressed only after Flpo-mediated recombination. Mice were monitored with MRI for tumor occurrence and received tamoxifen upon PDAC detection, leading to deletion of *Ptpn11* alleles in the epithelial tumor compartment of *FSF-CreRT^{positive}* mice. Mice without the *FSF-CreRT* allele served as controls. Tumor volume dynamics were continuously followed with weekly MRI. **b**, Representative magnetic resonance images of two exemplary mice taken at the indicated interval after tamoxifen administration to mice with established PDAC (green outline). The top panel depicts sequential images of a mouse from the *FSF-CreRT^{negative}* control cohort (SHP2 proficient, blue outline; $n=10$ animals with similar results) and the bottom panel depicts a mouse with loss of *Ptpn11* in the epithelial tumor compartment (SHP2 deficient, orange outline; $n=8$ animals with similar results). Scale bars, 1 cm. w, week. **c**, Quantification of pancreatic volume change over time after tumor detection and tamoxifen administration as measured by MRI. *Ptpn11^{fl/fl}* control cohort: $n=10$; *Ptpn11^{-/-}* deletion cohort: $n=8$. The dotted line indicates basal tumor volume at time of tamoxifen application. Volume-tracking curves for individual mice over the whole course of follow-up are available in Supplementary Fig. 8c. Mean \pm s.d. is shown. $*P=0.04$, paired, two-tailed Student's *t*-test. **d,e**, In vitro deletion of *Ptpn11* with 4-OH-tamoxifen (4-OH-T) in a PDAC cell line derived from a *FSF-CreRT^{positive}* mouse; ethanol (EtOH) served as the vehicle control. In panel **d**, short-term proliferation (5 days) of the resulting SHP2-proficient versus SHP2-deficient cell line pair was quantified. One experiment was performed with cells seeded as triplicates. Mean \pm s.d. is shown. $*P=0.048$, unpaired, two-tailed Student's *t*-test. In panel **e**, the loss of SHP2 was confirmed by immunoblot. Pull-down of RAS-GTP was performed with RAF-RBD agarose beads. Precipitates and input samples were analyzed using the respective antibodies (for an explanation of the labeling, see the legend for Fig. 2b). Numerical values indicate the ratio of densitometrically quantified signals from pull-down over input samples. β -Actin represents the loading control. One experiment was performed. Full scan images are shown in Supplementary Fig. 18c. **f**, Colony formation assays with YAPC and PANC-1 *PTPN11* wild-type (WT) versus knockout (KO) cells (two independent *PTPN11*-knockout cell lines are shown), treated with the MEK inhibitors selumetinib or trametinib at the indicated concentrations. Three independently repeated experiments were performed with similar results. **g**, Phospho-RTK Array with lysates from YAPC wild-type cells treated with selumetinib for 48 h versus untreated control (ctrl). RTKs with enhanced phosphorylation (antibodies are spotted in duplicate) in response to selumetinib are indicated with colored boxes. One experiment was performed. **h**, Immunoblot of lysates from YAPC wild-type and *PTPN11*-knockout clone #1.1 and #2.12 cells treated with selumetinib for the indicated hours. HSP90 served as the loading control. Three independently repeated experiments were performed with similar results. Full scan images are shown in Supplementary Fig. 18d. For the corresponding analysis with PANC-1 cells, see Supplementary Fig. 10g. **i**, In vitro co-inhibition of MEK (selumetinib) and SHP2 (GS493 or SHP099) in colony formation experiments with YAPC and PANC-1 human pancreatic cancer cell lines. Three independently repeated experiments were performed with similar results. For additional co-inhibition combinations and experiments with DAN-G, see Supplementary Fig. 11d; for quantification and calculation of combination index scores, see Supplementary Fig. 11e,f.

importantly, SHP2 is required to reestablish RAS signaling when downstream RAS effectors (for example, MEK) are inhibited. As RTK-mediated (context dependent: ERBB family³¹, ERBB family/PDGFR- α /AXL³² and fibroblast growth factor receptor 1 (FGFR1)³⁴)

resistance to MEK inhibition is a frequent and clinically relevant problem in PDAC and *KRAS*-mutant NSCLC, a therapeutic strategy comprising inhibitors of MEK with novel agents that target SHP2 could putatively overcome this clinical barrier. As an integrator of

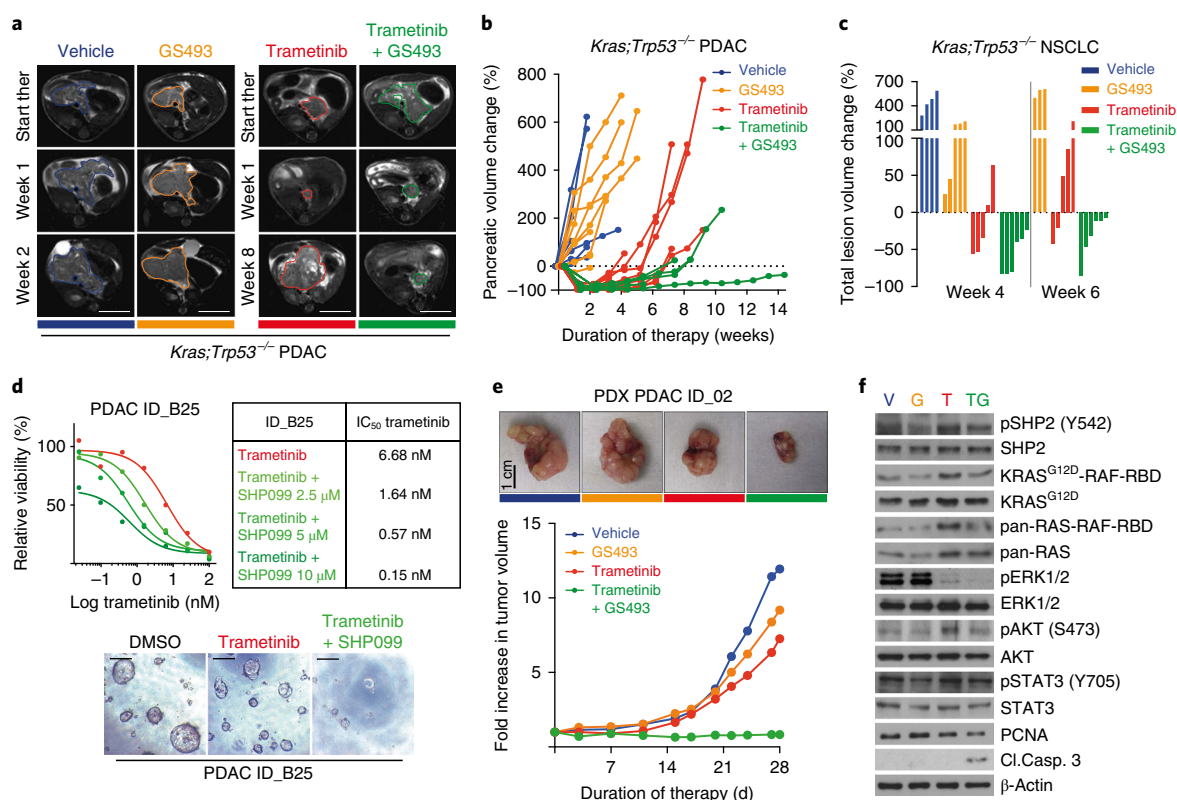


Fig. 4 | Dual MEK and SHP2 inhibition as a viable strategy to treat *KRAS*-mutant tumors. **a**, Representative MRI scan slices depicting PDAC tumor sections of *Kras;Trp53^{-/-}* mice treated with vehicle ($n=8$), GS493 ($n=11$), trametinib ($n=11$) or trametinib + GS493 ($n=13$) at the indicated time points (weeks) following the start of therapy (start ther), with similar results among the groups. Scale bars, 1 cm. **b**, MRI tracking of individual *Kras;Trp53^{-/-}* pancreatic volumes over the course of treatment. The number of mice is the same as in panel **a**. The dotted line indicates basal tumor volume at time of enrollment. Note that trametinib and the combination therapy trametinib + GS493 were associated with morbidity necessitating euthanasia before the occurrence of pancreatic volume relapse in a fraction of *Kras;Trp53^{-/-}* animals; for details, see the figure legend for Supplementary Fig. 14b. **c**, Waterfall plot depicting individual relative total lesion volumes after 4 and 6 weeks of therapy in *Kras;Trp53^{-/-}* AdCre NSCLC mice treated with vehicle ($n=5$), GS493 ($n=5$), trametinib ($n=6$) or trametinib + GS493 ($n=6$). **d**, Patient-derived ex vivo *KRAS*^{G12V} PDAC organoids treated with titrated trametinib, with or without three different concentrations of SHP099, for 6 days. Representative dose-response curves, tabular listing of IC₅₀ values for trametinib with or without increasing concentrations of SHP099 and representative bright-field micrographs of wells treated with DMSO control, trametinib 3 nM and trametinib 3 nM + SHP099 5 μM are shown. Scale bars, 100 μm. Three independently repeated experiments were performed with similar results. A second set of experiments with organoids established from a different PDAC is shown in Supplementary Fig. 16. **e**, Macroscopic photographs after 28 days of therapy and tumor volume tracking of PDAC tissue xenograft ID_02 (*KRAS*^{G12D}), treated as indicated. Each trial arm consisted of one mouse with two tumors implanted in the right and left flanks. The larger tumors are shown in the photographs and the volume-tracking plots. One experiment was performed. For additional experiments with two different PDAC tissue xenografts, see Supplementary Fig. 17a. **f**, Immunoblots and RAF-RBD agarose pull-downs of tissue lysates from PDAC ID_02 tissue xenograft tumors treated for 28 days as indicated. Pull-down of RAS-GTP was achieved using RAF-RBD agarose beads. Precipitates and input samples were analyzed using the respective antibodies (for an explanation of the labeling, see the legend for Fig. 2b). β-Actin served as the loading control. One experiment was performed. For uncropped images, including molecular weight markers, see Supplementary Fig. 18e. Cl.Casp. 3, cleaved caspase 3; G, GS493; T, trametinib; TG, trametinib + GS493; V, vehicle.

RTK-RAS signaling downstream of almost all RTKs, our findings, together with those from the accompanying manuscript by Mainardi et al.⁴¹, reveal that SHP2 may hold promise as a therapeutic target not only in RTK-driven tumors but also in *KRAS*-mutant tumors.

Methods

Methods, including statements of data availability and any associated accession codes and references, are available at <https://doi.org/10.1038/s41591-018-0024-8>.

Received: 5 July 2017; Accepted: 20 March 2018;
Published online: 28 May 2018

References

- Neel, B. G., Gu, H. & Pao, L. The 'Shp'ing news: SH2 domain-containing tyrosine phosphatases in cell signaling. *Trends Biochem. Sci.* **28**, 284–293 (2003).
- Xu, D. & Qu, C.-K. Protein tyrosine phosphatases in the JAK/STAT pathway. *Front. Biosci.* **13**, 4925–4932 (2008).
- Chan, G., Kalaitzidis, D. & Neel, B. G. The tyrosine phosphatase Shp2 (PTPN11) in cancer. *Cancer Metastasis Rev.* **27**, 179–192 (2008).
- Matozaki, T., Murata, Y., Saito, Y., Okazawa, H. & Ohnishi, H. Protein tyrosine phosphatase SHP-2: a proto-oncogene product that promotes Ras activation. *Cancer Sci.* **100**, 1786–1793 (2009).
- Chan, R. J. & Feng, G.-S. PTPN11 is the first identified proto-oncogene that encodes a tyrosine phosphatase. *Blood* **109**, 862–867 (2006).
- Bard-Chapeau, E. A. et al. Ptpn11/Shp2 acts as a tumor suppressor in hepatocellular carcinogenesis. *Cancer Cell* **19**, 629–639 (2011).
- Grossmann, K. S., Rosário, M., Birchmeier, C. & Birchmeier, W. The tyrosine phosphatase Shp2 in development and cancer. *Adv. Cancer Res.* **106**, 53–89 (2010).
- Chen, Y.-N. P. et al. Allosteric inhibition of SHP2 phosphatase inhibits cancers driven by receptor tyrosine kinases. *Nature* **535**, 148–152 (2016).
- Cox, A. D., Fesik, S. W., Kimmelman, A. C., Luo, J. & Der, C. J. Drugging the undruggable RAS: mission possible? *Nat. Rev. Drug Discov.* **13**, 828–851 (2014).

10. Almoguera, C. et al. Most human carcinomas of the exocrine pancreas contain mutant c-K-ras genes. *Cell* **53**, 549–554 (1988).
11. Zheng, J. et al. Pancreatic cancer risk variant in *LINC00673* creates a miR-1231 binding site and interferes with PTPN11 degradation. *Nat. Genet.* **48**, 747–757 (2016).
12. Schneeberger, V. E. et al. Inhibition of Shp2 suppresses mutant EGFR-induced lung tumors in transgenic mouse model of lung adenocarcinoma. *Oncotarget* **6**, 6191–6202 (2015).
13. Xu, J., Zeng, L.-F., Shen, W., Turchi, J. J. & Zhang, Z.-Y. Targeting SHP2 for EGFR inhibitor resistant non-small cell lung carcinoma. *Biochem. Biophys. Res. Commun.* **439**, 586–590 (2013).
14. Vogel, W., Lammers, R., Huang, J. & Ullrich, A. Activation of a phosphotyrosine phosphatase by tyrosine phosphorylation. *Science* **259**, 1611–1614 (1993).
15. Feng, G. S., Hui, C. C. & Pawson, T. SH2-containing phosphotyrosine phosphatase as a target of protein-tyrosine kinases. *Science* **259**, 1607–1611 (1993).
16. Lu, W., Shen, K. & Cole, P. A. Chemical dissection of the effects of tyrosine phosphorylation of SHP-2. *Biochemistry* **42**, 5461–5468 (2003).
17. Hingorani, S. R. et al. Preinvasive and invasive ductal pancreatic cancer and its early detection in the mouse. *Cancer Cell* **4**, 437–450 (2003).
18. Jackson, E. L. et al. Analysis of lung tumor initiation and progression using conditional expression of oncogenic K-ras. *Genes Dev.* **15**, 3243–3248 (2001).
19. Means, A. L. et al. Pancreatic epithelial plasticity mediated by acinar cell transdifferentiation and generation of nestin-positive intermediates. *Development* **132**, 3767–3776 (2005).
20. Aguirre, A. J. et al. Activated Kras and Ink4a/Arf deficiency cooperate to produce metastatic pancreatic ductal adenocarcinoma. *Genes Dev.* **17**, 3112–3126 (2003).
21. Bardeesy, N. et al. Both p16^{Ink4a} and the p19^{Arf}-p53 pathway constrain progression of pancreatic adenocarcinoma in the mouse. *Proc. Natl Acad. Sci. USA* **103**, 5947–5952 (2006).
22. Collisson, E. A. et al. A central role for RAF→MEK→ERK signaling in the genesis of pancreatic ductal adenocarcinoma. *Cancer Discov.* **2**, 685–693 (2012).
23. Blasco, R. B. et al. c-Raf, but not B-Raf, is essential for development of K-Ras oncogene-driven non-small cell lung carcinoma. *Cancer Cell* **19**, 652–663 (2011).
24. di Magliano, M. P. & Logsdon, C. D. Roles for KRAS in pancreatic tumor development and progression. *Gastroenterology* **144**, 1220–1229 (2013).
25. Srinivasan, L. et al. PI3 kinase signals BCR-dependent mature B cell survival. *Cell* **139**, 573–586 (2009).
26. Eser, S. et al. Selective requirement of PI3K/PDK1 signaling for Kras oncogene-driven pancreatic cell plasticity and cancer. *Cancer Cell* **23**, 406–420 (2013).
27. Lesina, M. et al. Stat3/Socs3 activation by IL-6 transsignaling promotes progression of pancreatic intraepithelial neoplasia and development of pancreatic cancer. *Cancer Cell* **19**, 456–469 (2011).
28. Schönhuber, N. et al. A next-generation dual-recombinase system for time- and host-specific targeting of pancreatic cancer. *Nat. Med.* **20**, 1340–1347 (2014).
29. Prahallad, A. et al. Unresponsiveness of colon cancer to BRAF(V600E) inhibition through feedback activation of EGFR. *Nature* **483**, 100–103 (2012).
30. Corcoran, R. B. et al. EGFR-mediated re-activation of MAPK signaling contributes to insensitivity of BRAF mutant colorectal cancers to RAF inhibition with vemurafenib. *Cancer Discov.* **2**, 227–235 (2012).
31. Sun, C. et al. Intrinsic resistance to MEK inhibition in KRAS mutant lung and colon cancer through transcriptional induction of ERBB3. *Cell Rep.* **7**, 86–93 (2014).
32. Pettazoni, P. et al. Genetic events that limit the efficacy of MEK and RTK inhibitor therapies in a mouse model of KRAS-driven pancreatic cancer. *Cancer Res.* **75**, 1091–1101 (2015).
33. Prahallad, A. et al. PTPN11 is a central node in intrinsic and acquired resistance to targeted cancer drugs. *Cell Rep.* **12**, 1978–1985 (2015).
34. Manchado, E. et al. A combinatorial strategy for treating KRAS-mutant lung cancer. *Nature* **534**, 647–651 (2016).
35. Infante, J. R. et al. A randomised, double-blind, placebo-controlled trial of trametinib, an oral MEK inhibitor, in combination with gemcitabine for patients with untreated metastatic adenocarcinoma of the pancreas. *Eur. J. Cancer* **50**, 2072–2081 (2014).
36. Jänne, P. A. et al. Selumetinib plus docetaxel compared with docetaxel alone and progression-free survival in patients with KRAS-mutant advanced non-small cell lung cancer: the SELECT-1 randomized clinical trial. *JAMA* **317**, 1844–1853 (2017).
37. Grosskopf, S. et al. Selective inhibitors of the protein tyrosine phosphatase SHP2 block cellular motility and growth of cancer cells in vitro and in vivo. *ChemMedChem* **10**, 815–826 (2015).
38. Garcia Fortanet, J. et al. Allosteric inhibition of SHP2: identification of a potent, selective, and orally efficacious phosphatase inhibitor. *J. Med. Chem.* **59**, 7773–7782 (2016).
39. Alagesan, B. et al. Combined MEK and PI3K inhibition in a mouse model of pancreatic cancer. *Clin. Cancer Res.* **21**, 396–404 (2015).
40. Caunt, C. J., Sale, M. J., Smith, P. D. & Cook, S. J. MEK1 and MEK2 inhibitors and cancer therapy: the long and winding road. *Nat. Rev. Cancer* **15**, 577–592 (2015).
41. Mainardi, S. et al. SHP2 is required for growth of KRAS-mutant non-small-cell lung cancer in vivo. *Nat. Med.* <https://doi.org/10.1038/s41591-018-0023-9> (2018).
42. Subramanian, A. et al. Gene set enrichment analysis: a knowledge-based approach for interpreting genome-wide expression profiles. *Proc. Natl Acad. Sci. USA* **102**, 15545–15550 (2005).

Acknowledgements

We thank G.-S. Feng (Department of Pathology, School of Medicine, and Molecular Biology, Division of Biological Sciences, University of California, San Diego, La Jolla, CA, USA) for sharing the *Ptpn11^{fl}* allele. We also thank R. F. Braren and D. C. Karampinos (both Institute of Radiology, Klinikum rechts der Isar, Technische Universität München) for providing the infrastructure and A. Gupta for help with the setup for MRI studies. This work was supported by grants from Deutsche Forschungsgemeinschaft (DFG AL1174/5-1 to H.A. and LE3222/1-1 to M.L.), Deutsche Krebshilfe (no. 111646 and no. 111464 to H.A.; Max Eder Program no. 111273 to M.R.), the Wilhelm Sander Stiftung (2014.052.1 to H.A.) and the Fundación Asociación Española Contra el Cáncer (to B.S.).

Author contributions

D.A.R., H.A. and G.J.H. conceived the study. D.A.R. conducted the animal experiments. D.A.R., A.B., D.K. and M.L. performed the histological scoring, immunohistochemistry and immunofluorescence. D.A.R., G.J.H., K.J.C., J.A., A.B. and E.A.Z.v.d.L. performed the immunoblotting. In vitro experiments with human PDAC cell lines including CRISPR-Cas9 knockout and reconstitution experiments were conducted by G.J.H. and E.A.Z.v.d.L. In vitro drug screening was done by K.J.C. and D.A.R. The oncogenic database analysis and GSEAs were performed by D.A.R. Maintenance of mouse colonies and genotyping were performed by D.A.R., K.J.C., J.A., D.K., K.G., K.N.D., S.M.W., M.L., A.F.K., A.B., M.K., E.K.-A. and L.S. M.P.L.-A., M.N. and W.B. synthesized GS493 and SHP099. K.J.C., Z.D., D.A.R. and M.R. performed the ex vivo organoid assay. D.S. generated mutant mouse alleles. M.E. and B.S. established the PDAC-PDX. D.A.R., G.J.H., K.J.C. and H.A. analyzed the data. D.A.R., G.J.H. and K.J.C. generated the figures. D.A.R. and H.A. wrote the original draft, with input from B.S. and G.J.H. Supervision was provided by H.A. Funding was provided by H.A., M.L., M.R., U.T.H., R.M.S., B.S. and W.B. All authors critically revised and approved the manuscript.

Competing interests

The authors declare no competing interests.

Additional information

Supplementary information is available for this paper at <https://doi.org/10.1038/s41591-018-0024-8>.

Reprints and permissions information is available at www.nature.com/reprints.

Correspondence and requests for materials should be addressed to H.A.

Publisher's note: Springer Nature remains neutral with regard to jurisdictional claims in published maps and institutional affiliations.

Methods

Mouse strains. *Kras^{LSL-G12D/+}* (*Kras^{tm1Ty1}*)¹⁸, *Ptfl1^{Cre-ex1}* (*Ptfl1^{tm1(Cre)Hnak}*)⁴³, *Ptpn11^{fl/fl}* (*Ptpn11^{tm1Gaf}*)⁴⁴, *Cdkn2a^{fl/fl}* (*Cdkn2a^{tm4Rdp}*)²⁰, *Trp53^{fl/fl}* (*Trp53^{tm1Bri}*)⁴⁵, *R26-LSL-Map2k1^{S218D/S222D}* (*Gt(ROSA)26Sor^{tm8(Map2k1,EGFP/Rsk)}*)²⁵, *R26-LSL-Pik3ca^{H1047R}* (*Gt(ROSA)26Sor^{tm2(Pik3ca)}*)²⁶, *Socs3^{fl/fl}* (*Socs3^{tm1Ayo}*)⁴⁶, *Kras^{FSF-G12D/+}* (*Kras^{tm1Dsa}*)²⁸, *Pdx-Flpo* (*Tg(Pdx1-flpo)#Dsa*)²⁸, *R26^{FSF-CAG-CreERT2}* (*Gt(ROSA)26Sor^{tm3(CAG-CreERT2)}*)²⁸ and *Trp53^{fl/fl}* (*Trp53^{tm1.1Dgk}*)⁴⁷ have been described previously. *R26^{td-EG}* dual Flp/Cre reporter mice were generated by and obtained from D.S. Strains were interbred to obtain the following compound mutants: *Kras^{LSL-G12D/+}*, *Ptfl1^{Cre-ex1}* (*Kras*); *Kras^{LSL-G12D/+}*, *Ptfl1^{Cre-ex1}*, *Ptpn11^{fl/fl}* (*Kras;Ptpn11^{-/-}*); *Kras^{LSL-G12D/+}*, *Ptfl1^{Cre-ex1}*, *Cdkn2a^{fl/fl}* (*Kras;Ink4a/Arf^{-/-}*); *Kras^{LSL-G12D/+}*, *Ptfl1^{Cre-ex1}*, *Cdkn2a^{fl/fl}*, *Ptpn11^{fl/fl}* (*Kras;Ink4a/Arf^{-/-};Ptpn11^{-/-}*); *Kras^{LSL-G12D/+}*, *Ptfl1^{Cre-ex1}*, *Trp53^{fl/fl}* (*Kras;Trp53^{+/-}*); *Kras^{LSL-G12D/+}*, *Ptfl1^{Cre-ex1}*, *Trp53^{fl/fl}* (*Kras;Trp53^{-/-}*); *Kras^{LSL-G12D/+}*, *Ptfl1^{Cre-ex1}*, *Trp53^{fl/fl}*, *Ptpn11^{fl/fl}* (*Kras;Trp53^{+/-};Ptpn11^{-/-}*); *Kras^{LSL-G12D/+}*, *Ptfl1^{Cre-ex1}*, *Trp53^{fl/fl}* (*Kras;Trp53^{-/-}*); *Kras^{LSL-G12D/+}*, *Ptfl1^{Cre-ex1}*, *Trp53^{fl/fl}*, *Ptpn11^{fl/fl}* (*Kras;Trp53^{-/-};Ptpn11^{-/-}*); *R26-LSL-Map2k1^{S218D/S222D}*, *Ptfl1^{Cre-ex1}*, *Ptpn11^{fl/fl}* or *Ptpn11^{fl/fl}* (*Map2k1;Ptpn11^{-/-}* and *Map2k1;Ptpn11^{-/-}*); *R26-LSL-Pik3ca^{H1047R}*, *Ptfl1^{Cre-ex1}*, *Ptpn11^{fl/fl}* or *Ptpn11^{fl/fl}* (*Pik3ca;Ptpn11^{+/-}* and *Pik3ca;Ptpn11^{-/-}*); *Kras^{LSL-G12D/+}*, *Ptfl1^{Cre-ex1}*, *Socs3^{fl/fl}*, *Ptpn11^{fl/fl}* or *Ptpn11^{fl/fl}* (*Kras;Socs3^{-/-};Ptpn11^{+/-}* and *Kras;Socs3^{-/-};Ptpn11^{-/-}*); *Kras^{FSF-G12D/+}*, *Pdx-Flpo*, *Trp53^{fl/fl}*, *R26^{FSF-CAG-CreERT2}* positive or negative, *R26^{td-EG}*, *Ptpn11^{fl/fl}* (*Kras;Trp53^{-/-};FSF-CreRT^{negative};Ptpn11^{fl/fl}* and *Kras;Trp53^{-/-};FSF-CreRT^{positive};Ptpn11^{fl/fl}*). Mice with pancreatic deletion of *Ptpn11* by *Ptfl1^{Cre-ex1}* were born at the expected Mendelian frequency and did not show any signs of impaired health, even with progressing age (data not shown). For mice of the lung tumor cohorts, nomenclature corresponds to those used for PDAC mice; yet, for NSCLC mice, *Ptfl1^{Cre-ex1}* was replaced by inhalation of AdCre. All mice were kept in a mixed genetic background. Genotypes were determined by PCR and gel electrophoresis at weaning and after death. NSG mice were obtained from Jackson Laboratory and bred under a Material Transfer Agreement with Klinikum rechts der Isar, Technische Universität München, Munich, Germany. All animal experiments and care were in accordance with the guidelines of institutional committees and approved by the local authority, Regierung von Oberbayern.

Inflammation-triggered accelerated pancreatic carcinogenesis. Chronic pancreatitis was induced by repetitive supramaximal stimulation with the cholecystokinin analogue cerulein (Sigma-Aldrich). Beginning at 8 weeks of age, *Kras* and *Kras;Ptpn11^{-/-}* mice received 5 daily intraperitoneal high-dose injections of the secretagogue (200 µg per kg body weight) followed by 2 days of rest for a period of 4 consecutive weeks. Animals were euthanized and analyzed at 13 weeks of age (see schematic in Supplementary Fig. 3e).

Pancreatic epithelial explants: isolation and in vitro transdifferentiation assay. Pancreatic epithelial explants from 4-week-old *Kras* and *Kras;Ptpn11^{-/-}* mice were established by slightly modified previously published protocols^{19,48}. In brief, the whole pancreas was collected and treated twice with 1.2 mg ml⁻¹ collagenase from *Clostridium histolyticum* (Sigma-Aldrich). Following three wash steps with McCoy's 5A medium (Sigma-Aldrich) containing 0.2 mg ml⁻¹ soybean trypsin inhibitor (Sigma-Aldrich) and 0.1% (w/v) BSA (Sigma-Aldrich), digested samples were filtered through a 100-µm cell strainer, resuspended in recovery medium (DMEM/F12 supplemented with 20% FBS and penicillin–streptomycin (100 U ml⁻¹, 100 µg ml⁻¹) (all from Life Technologies)) and allowed to recover for 1 h at 37 °C. Subsequently, cells were pelleted and either washed in ice-cold PBS and lysed for immunoblot analyses or resuspended in culture medium, consisting of Waymouth's MB 752/1 (Life Technologies) supplemented with 0.2 mg ml⁻¹ soybean trypsin inhibitor, 50 µg ml⁻¹ bovine pituitary extract (Life Technologies), insulin–transferrin–selenium (10 mg ml⁻¹, 5.5 mg ml⁻¹, 0.0067 mg ml⁻¹; Life Technologies), 0.1% FBS and penicillin–streptomycin. Rat tail collagen type I (Corning) at a final concentration of 2.5 mg ml⁻¹ was added and the suspension was immediately plated into wells precoated with 2.5 mg ml⁻¹ rat tail collagen type I. After solidification, culture medium was placed on top of the gel. Explants were treated with the indicated final concentrations of the SHP2 phosphatase inhibitor PHPS1 (Sigma-Aldrich) or vehicle control (DMSO) on day 1 and day 3 after plating. For quantification, acinar explants were seeded in triplicates. At day 5, all cell clusters were counted throughout whole wells and reported as a percentage of duct-like spheres and acinar clusters.

AdCre delivery and NSCLC model. Sporadic expression of Cre in mouse lungs was achieved by transnasal inhalation of engineered adenovirus (University of Iowa, Viral Vector Core) as previously described⁴⁹. Following anesthesia with intraperitoneal medetomidine (0.5 mg per kg), midazolam (5 mg per kg) and fentanyl (0.05 mg per kg), a final volume of 60 µl MEM carrying 5 × 10⁷ p.f.u. calcium phosphate co-precipitated AdCre was dispensed dropwise over the left nostril of 6–8-week-old mice until inhaled in its entirety. Analgo-sedation was antagonized by subcutaneous atipamezole (2.5 mg per kg), flumazenil (0.5 mg per kg) and naloxone (1.2 mg per kg), and mice were monitored under a heat lamp in the biosafety hood until completely recovered.

Dual-recombinase system. Sequential genetic manipulation of the murine pancreas was accomplished through a combined Flpo-FRT and Cre-loxP system as previously reported²⁸. Pancreatic tumors were initiated by *Pdx-Flpo*-mediated

recombination of *Kras^{FSF-G12D/+}* and *Trp53^{fl/fl}* alleles and expressed a tamoxifen-inducible Cre-recombinase from the R26 locus (*R26^{FSF-CAG-CreERT2}*). Mice were monitored by MRI, as described below, and received 3 mg tamoxifen (in 150 µl corn oil; Sigma-Aldrich) per oral gavage on 3 consecutive days when tumor volumes had reached 50–450 mm³, resulting in excision of the floxed *Ptpn11* alleles. Mice lacking the *R26^{FSF-CAG-CreERT2}* allele underwent the same procedure and served as controls. Dual recombination was confirmed by a double fluorescence/bioluminescence reporter allele (*R26^{td-EG}*), which, upon Flpo-mediated recombination, expresses E/GFP and firefly luciferase, and after Cre-mediated recombination, loses the E/GFP/firefly sequences and expresses tdTomato and Renilla luciferase.

For in vitro deletion of *Ptpn11*, a primary ex vivo PDAC cell line was established from a moribund *Kras;Trp53^{-/-};FSF-CreRT^{positive};Ptpn11^{fl/fl}* mouse and was treated daily with 2 µM 4-OH-tamoxifen (Sigma-Aldrich) or with vehicle control (pure ethanol) for 6 consecutive days. Loss of SHP2 was verified by immunoblotting.

MRI. MRI experiments for *Kras;Trp53^{-/-}*, *Kras;Trp53^{-/-}* Ad-Cre, *Kras;Trp53^{-/-};FSF-CreRT^{negative};Ptpn11^{fl/fl}* and *Kras;Trp53^{-/-};FSF-CreRT^{positive};Ptpn11^{fl/fl}* mice were initiated at an age of 28–35 days and were repeated weekly as described previously⁴⁸. Sedation was performed via continuous inhalation of 2% isoflurane (Abbott) in O₂ using a veterinary anesthesia system (Vetland Medical). Body temperature was maintained and monitored, and eyes were protected by eye ointment. Image acquisition was achieved using a microscopy surface coil inside a 3.0 T clinical device (Philips) and an axial multislice T2-weighted turbo spin echo sequence (resolution: 0.3 × 0.3 × 0.7 mm³, 30 slices, echo time = 90 ms, repetition time > 3 s). Solid tumor volumes were calculated using OsiriX Lite DICOM viewer (Pixmeo) by summing truncated pyramid volumes between tumor areas on vicinal slices. On average, *Kras;Trp53^{-/-}* mice at age 38 days (95% confidence interval (CI): 35–40 days) met inclusion criteria for the therapy trial with a mean pancreatic volume of 319 mm³ (95% CI: 261–377 mm³). *Kras;Trp53^{-/-}* AdCre mice were enrolled for treatment at a mean time post-AdCre inhalation of 60 days (95% CI: 56–63 days), with a mean lesion load of 99 mm³ (95% CI: 55–142 mm³). Dosing and schedule of drug administration are detailed below.

Human PDAC specimens and patient-derived tissue xenografts. PDAC tissues were obtained from patients who underwent surgical resection at the Koç University Hospital, Istanbul, Turkey (M.E.). All patients provided written informed consent. For the xenograft therapy trial, samples (all KRAS^{G12D}) were procured and expanded in vivo under a Material Transfer Agreement at the Universidad Autónoma de Madrid and with approval of the ethical review board (CEI 60-1057-A068) and the Comunidad de Madrid (Red PROEX 335/14). Each sample was cut into approximately 200–300-mm³ pieces. Fragments were coated in Matrigel basement membrane matrix (Corning) and implanted in subcutaneous pockets in the posterior flanks of 8-week-old NSG mice. Tumors were passaged for 2–3 generations before initiation of treatment trials. Volumes were evaluated every 2–3 days by caliper measurements and the approximate volume (V) of the mass was estimated using the formula V = D × d²/2, with D being the major tumor axis and d being the minor tumor axis. Established tumors (average volume at inclusion: 150–300 mm³) were randomly assigned to trial arms and treated as specified below. Experiments were terminated once vehicle control tumors reached a critical size at the ethical end point (V = 2,000–4,000 mm³). End-of-treatment tumor material was snap frozen in liquid nitrogen and stored at –80 °C for protein analysis.

Human pancreatic cancer cell line xenografts. Cells (numbers as indicated) were suspended in 100 µl of a 1:1 mixture of DMEM and Matrigel (Corning) and injected subcutaneously into the flanks of NSG mice. Tumor volume was monitored as indicated above for the tissue xenografts. Therapy was initiated after tumors had reached a volume of 50–100 mm³. For drug dosing and schedule, see below.

Drugs and inhibitors. Trametinib, selumetinib, picitilisib, oxaliplatin and paclitaxel were purchased from Selleckchem, gemcitabine was provided by the Hospital Pharmacy of Klinikum Rechts der Isar (Technische Universität München), and GS493 and SHP099 were synthesized and kindly provided by M.N., Medicinal Chemistry, Leibniz-Forschungsinstitut für Molekulare Pharmakologie, Berlin, Germany. PHPS1 (ref.⁵⁰) was obtained from Sigma-Aldrich. Drugs were dissolved in DMSO to yield 5–50 mM stock solutions and stored at –80 °C.

In vivo therapy dosing. For in vivo application in *Kras;Trp53^{-/-}* and NSG mice, trametinib was diluted in 0.5% hydroxypropyl methylcellulose (Sigma-Aldrich) and 0.2% Tween 80 (Sigma-Aldrich) in water. GS493 was dissolved in Kolliphor EL (Sigma-Aldrich) and applied in an emulsion of 10% Kolliphor EL, 10% ethanol and water. Trametinib (1 mg per kg) was administered by oral gavage (*Kras;Trp53^{-/-}* mice: every other day; NSG mice: 5 days on, 2 days off), whereas GS493 was injected intraperitoneally (30 mg per kg, same schedule)⁵¹.

Histology and immunohistochemistry. Tissue specimens were either snap frozen in OCT (Sakura Finetek) or fixed in 4% buffered paraformaldehyde,

dehydrated and embedded in paraffin wax. OCT (optimal cutting temperature compound) cryosections (10 μm) were used for lineage tracing fluorescence microscopy after brief fixing in ethanol and nuclear staining with DAPI (Vector Laboratories). Formalin-fixed paraffin-embedded sections of 3 μm were stained with H&E, Sirius Red or used for immunohistochemical studies.

Immunohistochemistry was performed on murine and human formalin-fixed paraffin-embedded sections using avidin-biotin enhancement (Vector Laboratories). The following antibodies were used: SHP2 (3397; 1:200), pERK1/2 (4376; 1:100), pSTAT3 Y705 (9145; 1:100), pAKT (3787; 1:50), cleaved caspase 3 (9661; 1:200) from Cell Signaling, pSHP2 Y542 (ab62322; 1:500) and Ki67 (ab15580; 1:1,000) from Abcam, cyclin D1 (SP4; 1:100) from Thermo Scientific and Amylase (46657; 1:500) from Santa Cruz. Slides were developed with DAB (3,3'-diaminobenzidine, Vector Laboratories) and counterstained with hematoxylin. Image acquisition was achieved on a Zeiss AxioImager.A1 microscope. Quantitative analyses of tumor areas and immunohistochemistry staining were performed with Axiovision (Zeiss) and ImageJ softwares.

Cell culture and cell lines. Primary murine tumor cell lines were established from chopped pieces of explanted tumors without enzymatic digestion. All murine cell lines were routinely cultured in DMEM supplemented with 10% FBS and penicillin-streptomycin (100 U ml⁻¹, 100 μg ml⁻¹) (all Life Technologies). PANC-1 (KRAS^{G12D}; p53^{R273H}), YAPC (KRAS^{G12V}; p53^{H179R}; SMAD4^{R156S/23}), DAN-G (KRAS^{G12V}; p53^{GEYFTFLQV3256}; CDKN2A^{P0}), CAPAN-1 (KRAS^{G12V}; p53^{A159V}; SMAD4^{S344*}; CDKN2A^{P0}), CAPAN-2 (KRAS^{G12V}; TP53^{c-375G>*}), ASPC-1 (KRAS^{G12D}; p53^{C135fs>35}; SMAD4^{R100T}; CDKN2A^{P.L78fs>41}), SU86.86 (KRAS^{G12D}; p53^{G245S}; CDKN2A^{P0}), COLO357 (KRAS^{G12D}), T3M4 (KRAS^{Q61H}; p53^{Y220C}) and BXPC3 (KRAS^{WT}; p53^{Y220C}; CDKN2A^{P0}), SMAD4^{L165del1659}) were purchased from the Deutsche Sammlung von Mikroorganismen und Zellkulturen GmbH (DSMZ). H358 (KRAS^{G12C}), H2170 (KRAS^{WT}; p53^{R158H}; CDKN2A^{P0}) and H1975 (KRAS^{WT}; EGFR^{L858R/p.T790M}; PIK3CA^{R.G18D}; p53^{R273H}; CDKN2A^{P.E69*}) were a kind gift from P. Jost (Klinikum rechts der Isar, Technische Universität München). Mutational status of the cell lines was compiled from the American Type Culture Collection (ATCC), Catalogue of Somatic Mutations in Cancer (COSMIC; Wellcome Trust Sanger Institute) and Cancer Cell Line Encyclopedia (CCLE, Broad Institute) databases. PANC-1 cells were cultured in DMEM, all other human cell lines in RPMI1640 (Life Technologies), supplemented with 10% FBS and penicillin-streptomycin (100 U ml⁻¹, 100 μg ml⁻¹). All cells were kept at 37 °C in a humidified incubator with 5% CO₂.

Plasmids, cloning and transfection. To generate CRISPR-Cas9 *PTPN11* constructs, the pX458 vector was used to clone in guide RNAs (gRNAs) targeting the *PTPN11* gene. The oligonucleotide sequences for both *PTPN11* gRNAs are as follows: *PTPN11* gRNA 1: forward: CACCGGAGGAACATGACATCGCGG, reverse: AAACCCGGATGTCATGTTCTCC; *PTPN11* gRNA 2: forward: CCACGAACATGACATCGCGAGGTG, reverse: AAACCACCTCCGGATGTCATGTTTC. Forward and reverse oligos for each gRNA were annealed and ligated into the BbsI-digested pX458 vector. Target cells were subsequently transfected with the pX458-*PTPN11*-gRNA plasmids using polyethylenimine. Positively transfected cells expressing GFP were then FACS sorted as single cells in 96-well plates. Clones were allowed to grow out and analyzed for SHP2 status. SHP2-knockout clones were then named after the gRNA and clone name, for example, YAPC #1.1 refers to gRNA 1, clone 1.

For the SHP2^{WT} and SHP2^{C459S} reconstitution experiments, the pCMV-GFP plasmid was available in the Birchmeier laboratory, and pCMV-SHP2-WT (8381) and pCMV-SHP2-C459S (8382) plasmids were purchased from AddGene. SHP2-knockout clones were transfected with pCMV-GFP, pCMV-SHP2-WT or pCMV-SHP2-C459S using polyethylenimine. Subsequently, transfected cells were selected with G418 (800 μg ml⁻¹ G418 until non-transfected control cells were dead, then maintained in 200 μg ml⁻¹ G418), and clones that formed were picked and analyzed for SHP2 expression.

For the SHP2^{E76A} reconstitution experiment, pBp-SHP2-E76A was purchased from Addgene (8331); the control vector pBp-GFP was available in the Birchmeier laboratory. Using polyethylenimine, the plasmids were transfected in AmphoPack-293 cells (631505, Takara) to produce amphotrophic viral particles. The virus-containing supernatant was subsequently used to transduce PANC-1 *PTPN11*-knockout #2.6 cells in three consecutive rounds of infection. The viral supernatant was supplemented with 8 μg ml⁻¹ polybrene. Infected cells were then selected in 2 μg ml⁻¹ puromycin.

Phosphatase assay. To measure SHP2 phosphatase activity, sub-confluent cell lines (YAPC and PANC-1) were serum starved (0.1% FBS) for 18 h and then treated with selumetinib (or left untreated) in full-growth medium (10% FBS) for 24 h. Cells were then washed once with cold PBS and lysed on ice in cold PTP lysis buffer (25 mM HEPES, pH 7.4, 150 mM NaCl, 1 mM dithiothreitol, 2 mM EDTA, 0.5% Triton X-100 and 1:50 diluted protease inhibitor cocktail (Serva)). Cell lysate supernatants (2 mg each) were pre-cleared with Pierce Protein A/G Agarose (Life Technologies) for 1 h, transferred to a new tube and incubated with SHP2 antibody (3397, Cell Signaling) or a rabbit IgG control (Santa Cruz) at 4 °C on a rotator. Protein A/G Agarose beads (60 μl each, 50% slurry) were added for an additional

2 h. Following a brief centrifugation, supernatants were collected for immunoblot analysis of immunoprecipitation efficiency. Immunoprecipitates were washed twice with PTP lysis buffer, twice with reaction buffer (25 mM HEPES, pH 7.4, 50 mM NaCl, 1 mM dithiothreitol and 0.05% Triton X-100), followed by resuspension in 100 μl reaction buffer containing 50 μM DiFMUP (Biomol) and incubated at room temperature for 20 min. After a brief centrifugation, supernatants were transferred into a 96-well plate and the dephosphorylated DiFMUP (DiFMU) fluorescence signal was measured at 358 nm excitation and 455 nm emission on a FLUOstar OPTIMA plate reader. The remaining immune complexes were used for immunoblotting analysis of the SHP2 protein.

Proliferation assays. Cells were seeded in triplicate into 6-well plates and trypsinized, collected and counted using trypan blue and Countess Automated Cell Counter (Invitrogen) at indicated time points.

In vitro drug screening and colony formation assays. Cells were seeded into 6-, 12- or 24-well plates (20 \times 10³, 5 \times 10³ or 1–4 \times 10³ cells per well, respectively) and allowed to adhere overnight in regular growth media. Cells were cultured in the absence or presence of drugs, as indicated, and refreshed every 2–3 days until the end of the experiment (on average, after 10–14 days). For each independent experiment, the different conditions were simultaneously fixed in 3.5% formaldehyde or 6% glutaraldehyde and subsequently stained with 0.1% crystal violet and digitalized on an image scanner. Relative growth was quantified by densitometry. All experiments were performed at least twice and representative results are shown.

Quantitative analysis of drug synergy. Drug synergy was calculated using CompuSyn software (version 1.0), which is based on the median-effect principle and the combination index–isobologram theorem³². CompuSyn software generates combination index values, where combination index < 0.75 indicates synergism, combination index = 0.75–1.25 indicates additive effects and combination index > 1.25 indicates antagonism. Following the instructions of the software, drug combinations at non-constant ratios were used to calculate the combination index in our study.

Patient-derived ex vivo PDAC organoid culture, treatment and read-out. Ex vivo organoids from resected human PDAC samples were generated and expanded as described previously³³, with minor adaptations. To achieve conditions for high-throughput drug screening, single cells were isolated from established organoids by enzymatic digestion and gentle mechanical force. Cell-Matrigel suspensions were delivered into 96-well plates (1 \times 10³ cells per well) and single cells readily reformed organoids upon replating. After 24 h, titration treatments were initiated, and cell viability was measured 5 days after drug addition via CellTiter-Glo 3D Viability Assay (Promega) luminescence on a FLUOstar OPTIMA microplate reader (BMG Labtech). All donors provided written informed consent and experiments were approved by the local ethics committee of the Faculty of Medicine, Technische Universität München, Projects 1946/07 and 207/15.

Western blotting, RAS-RAF-RBD pulldown and phospho-arrays. Tissues were immediately snap frozen in liquid nitrogen at the time of organ harvest. Tissues or cells were lysed in Mg²⁺ lysis buffer (125 mM HEPES, pH 7.5, 750 mM NaCl, 5% Igepal CA-630, 50 mM MgCl₂, 5 mM EDTA and 10% glycerol; Millipore) or in RIPA buffer (50 mM Tris pH 7.4, 150 mM NaCl, 1% NP-40, 0.1% SDS and 0.5% sodium deoxycholate) supplemented with protease inhibitor (Serva or Roche) and phosphatase inhibitor cocktails (Serva or Sigma-Aldrich). Protein concentrations were determined by Bradford assay (Bio-Rad). For western blotting, proteins were separated by SDS-PAGE in Laemmli buffer, transferred to nitrocellulose or polyvinylidene difluoride (PVDF) membranes and detected with the following antibodies: ERK1/2 (9102 or sc-93/sc-154) and SHP2 (3397 or sc-280) were from Cell Signaling or Santa Cruz. AKT (9272), pAKT S473 (9271), cleaved caspase 3 (9661), insulin-like growth factor receptor- β (IGFR- β ; 3027), pIGFR- β Y1135/1136 (3024), MET (#8198), pMET Y1234/1235 (3126), RAS^{G12D}-mutant specific (14429), STAT3 (9139), and pSTAT3 Y705 (9131) were purchased from Cell Signaling. Heat shock protein 90 (HSP90; sc-7947) and proliferating cell nuclear antigen (sc-56) were from Santa Cruz, and pSHP2 Y542 (ab51174) and KRAS (ab180772) were from Abcam. pan-RAS (05-516) was acquired from Millipore and β -actin-horseradish peroxidase (A3854) from Sigma-Aldrich. Signal detection was performed using horseradish peroxidase-conjugated secondary antibodies and an enhanced chemiluminescent reagent (Amersham, GE Healthcare) followed by signal read-out in a Fusion SL-3 imaging system (Vilber) or by development on film. RAS-GTP levels were measured using the RAS Activation Assay Kit from Millipore (17-218) per manufacturer's instructions. Briefly, fresh pancreatic tissue or PDAC cell lines were lysed in ice-cold Mg²⁺ lysis buffer and equal amounts of protein were incubated with RAF-1-RBD agarose beads for 45 min at 4 °C on a rotator. After three washing steps, beads were suspended in Laemmli-reducing sample buffer, subjected to SDS-PAGE and blotted on nitrocellulose membranes. Detection was performed with the indicated antibodies. The human Phospho-Kinase and Phospho-RTK Arrays were purchased from R&D Systems (ARY003B and ARY001B, respectively) and

were used according to the provided protocols. As the Phospho-Kinase Array is validated only for human samples, probable cross-reaction of most of the spotted antibodies with corresponding murine antigens was confirmed by the manufacturer. Densitometric quantification of immunoblots or phospho-arrays was performed with ImageJ software.

Publicly available transcriptomic databases. Comparative transcriptomic analyses between the normal pancreas and pancreatic cancer were performed, integrating all available data sets on the oncogenomic web-portal OncoPrint. Correlation of *PTPN11* expression with patient survival in pancreatic adenocarcinoma and *KRAS*-mutant lung adenocarcinoma was analyzed in TCGA RNA-seq PAAD and LUAD data sets, which are accessible via the University of California Santa Cruz (UCSC), Xena public data hub.

Microarray data analysis. Fresh pancreatic tissue samples from 9-week-old *Kras* and *Kras;Ptpn11*^{-/-} mice were homogenized and lysed in RLT lysis buffer (Qiagen) supplemented with 1:100 2-mercaptoethanol (Sigma-Aldrich). Sample processing and Affymetrix microarray hybridization (GeneChip (*Mus musculus*) Mouse Gene 1.0 ST arrays) were carried out at a genomics core facility: the Center of Excellence for Fluorescent Bioanalytics (KFB, University of Regensburg, Germany). Gene expression microarray data were analyzed using GSEA software provided by the Broad Institute, Cambridge, MA, USA, as previously described¹². A false discovery rate (*q* value) of >0.25 and a nominal *P* value of >0.05 were considered statistically significant.

Statistical analysis. Kaplan–Meier survival curves were calculated from all individual survival times of mice from the different genotype cohorts. Curves were compared by log-rank (Mantel–Cox) test to detect significant differences between the groups. For image quantifications and cell proliferation assays, significance was assayed by unpaired, two-tailed Student's *t*-test or Mann–Whitney test for comparison of two groups and by one-way analysis of variance (ANOVA) with post-hoc Tukey's test for more than two groups (variances were first examined by *F*-test or the Brown–Forsythe test, respectively); ****P* < 0.001; ***P* < 0.01; **P* < 0.05. Statistical analysis was performed with GraphPad PRISM 7.0 software. Data are represented as dot plots with bar graphs for mean ± standard deviation (s.d.) or standard error of the mean (s.e.m.), as indicated, or as box-and-whisker plots with boxes ranging from the 25th to 75th percentile, whiskers from minimum to maximum and the median as the center.

Reporting summary. Further information on experimental design is available in the Nature Research Reporting Summary linked to this article.

Data availability. Microarray hybridization raw data used for GSEAs (represented in Fig. 2 and Supplementary Fig. 6) were deposited in the EMBL-EBI ArrayExpress database under accession number E-MTAB-6399 (<https://www.ebi.ac.uk/arrayexpress/experiments/E-MTAB-6399>).

References

- Nakhai, H. et al. Ptf1a is essential for the differentiation of GABAergic and glycinergic amacrine cells and horizontal cells in the mouse retina. *Development* **134**, 1151–1160 (2007).
- Zhang, E. E., Chapeau, E., Hagihara, K. & Feng, G.-S. Neuronal Shp2 tyrosine phosphatase controls energy balance and metabolism. *Proc. Natl Acad. Sci. USA* **101**, 16064–16069 (2004).
- Marino, S., Vooijs, M., van Der Gulden, H., Jonkers, J. & Berns, A. Induction of medulloblastomas in p53-null mutant mice by somatic inactivation of Rb in the external granular layer cells of the cerebellum. *Genes Dev.* **14**, 994–1004 (2000).
- Yasukawa, H. et al. IL-6 induces an anti-inflammatory response in the absence of SOCS3 in macrophages. *Nat. Immunol.* **4**, 551–556 (2003).
- Lee, C.-L. et al. Generation of primary tumors with Flp recombinase in FRT-flanked p53 mice. *Dis. Model. Mech.* **5**, 397–402 (2012).
- Mazur, P. K. et al. Combined inhibition of BET family proteins and histone deacetylases as a potential epigenetics-based therapy for pancreatic ductal adenocarcinoma. *Nat. Med.* **21**, 1163–1171 (2015).
- DuPage, M., Dooley, A. L. & Jacks, T. Conditional mouse lung cancer models using adenoviral or lentiviral delivery of Cre recombinase. *Nat. Protoc.* **4**, 1064–1072 (2009).
- Hellmuth, K. et al. Specific inhibitors of the protein tyrosine phosphatase Shp2 identified by high-throughput docking. *Proc. Natl Acad. Sci. USA* **105**, 7275–7280 (2008).
- Lan, L. et al. Shp2 signaling suppresses senescence in PyMT-induced mammary gland cancer in mice. *EMBO J.* **34**, 1493–1508 (2015).
- Chou, T.-C. Drug combination studies and their synergy quantification using the Chou–Talalay method. *Cancer Res.* **70**, 440–446 (2010).
- Boj, S. F. et al. Organoid models of human and mouse ductal pancreatic cancer. *Cell* **160**, 324–338 (2015).

Life Sciences Reporting Summary

Nature Research wishes to improve the reproducibility of the work that we publish. This form is intended for publication with all accepted life science papers and provides structure for consistency and transparency in reporting. Every life science submission will use this form; some list items might not apply to an individual manuscript, but all fields must be completed for clarity.

For further information on the points included in this form, see [Reporting Life Sciences Research](#). For further information on Nature Research policies, including our [data availability policy](#), see [Authors & Referees](#) and the [Editorial Policy Checklist](#).

▶ Experimental design

1. Sample size

Describe how sample size was determined.

Investigating the role of SHP2/PTPN11 in carcinogenesis and tumor maintenance of KRAS mutant tumors using genetically engineered mouse models was performed as an exploratory study making sample size analysis inappropriate. Sample sizes for in vivo therapy trials were estimated by the Resource Equation Method.

2. Data exclusions

Describe any data exclusions.

No data were excluded from the analyses.

3. Replication

Describe whether the experimental findings were reliably reproduced.

All attempts at replication yielded similar results.

4. Randomization

Describe how samples/organisms/participants were allocated into experimental groups.

Where applicable (in vivo therapy trials), animals were allocated to groups in an unbiased manner by assigning the treatment arm to single mice before determination of tumor volume (MRI for endogenous PDAC/NSCLC; caliper measurement for subcutaneous xenografts).

5. Blinding

Describe whether the investigators were blinded to group allocation during data collection and/or analysis.

For the treatment studies, drug administration was only possible in an unblinded fashion, but tumor volume measurements/analysis were performed by a blinded scientist.

Note: all studies involving animals and/or human research participants must disclose whether blinding and randomization were used.

6. Statistical parameters

For all figures and tables that use statistical methods, confirm that the following items are present in relevant figure legends (or in the Methods section if additional space is needed).

n/a Confirmed

- The exact sample size (n) for each experimental group/condition, given as a discrete number and unit of measurement (animals, litters, cultures, etc.)
- A description of how samples were collected, noting whether measurements were taken from distinct samples or whether the same sample was measured repeatedly
- A statement indicating how many times each experiment was replicated
- The statistical test(s) used and whether they are one- or two-sided (note: only common tests should be described solely by name; more complex techniques should be described in the Methods section)
- A description of any assumptions or corrections, such as an adjustment for multiple comparisons
- The test results (e.g. P values) given as exact values whenever possible and with confidence intervals noted
- A clear description of statistics including central tendency (e.g. median, mean) and variation (e.g. standard deviation, interquartile range)
- Clearly defined error bars

See the web collection on [statistics for biologists](#) for further resources and guidance.

► Software

Policy information about [availability of computer code](#)

7. Software

Describe the software used to analyze the data in this study.

GraphPad PRISM 7.0c

For manuscripts utilizing custom algorithms or software that are central to the paper but not yet described in the published literature, software must be made available to editors and reviewers upon request. We strongly encourage code deposition in a community repository (e.g. GitHub). [Nature Methods guidance for providing algorithms and software for publication](#) provides further information on this topic.

► Materials and reagents

Policy information about [availability of materials](#)

8. Materials availability

Indicate whether there are restrictions on availability of unique materials or if these materials are only available for distribution by a for-profit company.

Unique materials used are readily available from the authors (SHP2 inhibitor: GS493).

9. Antibodies

Describe the antibodies used and how they were validated for use in the system under study (i.e. assay and species).

For immunohistochemistry:
 SHP2 (#3397; 1:200), pERK1/2 (#4376; 1:100), pSTAT3 Y705 (#9145; 1:100), pAKT (#3787; 1:50), Cleaved Caspase 3 (#9661; 1:200) from Cell Signaling, pSHP2 Y542 (ab62322; 1:500) and Ki67 (ab15580; 1:1000) from Abcam, Cyclin D1 (SP4; 1:100) from Thermo Scientific, and Amylase (#46657; 1:500) from Santa Cruz. All antibodies were validated for IHC application by the manufacturer as stated in the respective datasheets, except for SHP2 #3397 from Cell Signaling, which was established and validated using murine conditional SHP2-knockout pancreata as negative controls (cf. Supplementary Fig. 2a).

For immunoblotting:
 ERK1/2 (#9102 or sc-93/sc-154) and SHP2 (#3397 or sc-280) were from Cell Signaling or Santa Cruz. AKT (#9272), pAKT S473 (#9271), Cleaved Caspase 3 (#9661), IGF1R (#3027), pIGFR Y1135/1136 (#3024), MET (#8198), pMET Y1234/1235 (#3126), RASG12D mutant specific (#14429), STAT3 (#9139), and pSTAT3 Y705 (#9131) were purchased from Cell Signaling. HSP90 (sc-7947) and PCNA (sc-56) were from Santa Cruz, pSHP2 Y542 (ab51174 and ab62322) was from Abcam. pan-RAS (05-516) was acquired from Millipore and β -actin-HRP (A3854) from Sigma-Aldrich. All antibodies are validated by the manufacturer for the relevant applications and species analyzed.

10. Eukaryotic cell lines

a. State the source of each eukaryotic cell line used.

Murine cell lines:

Primary murine tumor cell lines were established from chopped pieces of explanted tumors without enzymatic digestion.

Human cell lines:

PANC-1, YAPC, DAN-G, CAPAN-1, CAPAN-1, ASPC-1, SU86.86, COLO357, T3M4 and BXPC3 were purchased from the Deutsche Sammlung von Mikroorganismen und Zellkulturen GmbH (DSMZ). H358, H2170 and H1975 were a kind gift from P. Jost (Klinikum rechts der Isar, Technische Universität München, Munich, Germany)

b. Describe the method of cell line authentication used.

Human cell lines were acquired as stated above and not further authenticated.

c. Report whether the cell lines were tested for mycoplasma contamination.

Cells were tested for mycoplasma contamination by PCR.

d. If any of the cell lines used are listed in the database of commonly misidentified cell lines maintained by [ICLAC](#), provide a scientific rationale for their use.

No commonly misidentified cell lines were used.

► Animals and human research participants

Policy information about [studies involving animals](#); when reporting animal research, follow the [ARRIVE guidelines](#)

11. Description of research animals

Provide details on animals and/or animal-derived materials used in the study.

All interbred mouse strains were kept in a mixed genetic background (C57BL6/FVB/129) and housed in a SPF facility with 12h-12h light/dark cycle and ad libitum access to food and water. Both sexes were included in the analyses.

KrasLSL-G12D/+ (Krstm1Tyj), Ptf1a+/Cre-ex1 (Ptf1atm1(cre)Hnak), Ptpn11fl/fl (Ptpn11tm1Gsf), Cdkn2af1/fl (Cdkn2atm4Rdp), Trp53fl/fl (Trp53tm1Brn), R26-LSL-Map2k1S218D/S222D (Gt(ROSA)26Sortm8(Map2k1*,EGFP)Rsky), R26-LSL-Pik3caH1047R (Gt(ROSA)26Sortm2(Pik3ca*)Das), Socs3fl/fl (Socs3tm1Ayos), KrasFSF-G12D/+ (Krstm1Dsa), Pdx-Flpo (Tg(Pdx1-flpo)#Dsa), R26FSF-CAG-CreERT2 (Gt(ROSA)26Sortm3(CAG-Cre/ERT2)Dsa), and Trp53frt/frt (Trp53tm1.1Dgk) have been described before. R26td-EG dual Flp/Cre reporter mice were generated by the authors.

NSG-mice were obtained from Jackson Laboratory and bred under a MTA with Klinikum rechts der Isar, Technische Universität München.

Policy information about [studies involving human research participants](#)

12. Description of human research participants

Describe the covariate-relevant population characteristics of the human research participants.

The study did not involve human research participants.